FULL-SCALE PERFORMANCE ASSESSMENT OF AIRCRAFT SECONDARY SANDWICH STRUCTURE USING THERMOELASTIC STRESS ANALYSIS

D. A. Crump[1], J. M. Dulieu-Barton[1] and J. Savage[2]
[1] School of Engineering Sciences, University of Southampton, Highfield, Southampton, SO17 1BJ, UK, email: dac400@soton.ac.uk
[2] GE Aviation, Kings Avenue, Hamble-Le-Rice, Hampshire, SO31 4NF, UK

SUMMARY

The use of resin film infusion (RFI) has been proven to reduce the cost of production of aircraft secondary sandwich structure. In this paper thermoelastic stress analysis (TSA) is used to assess the performance of full scale aircraft sandwich structure panels produced using both the conventional autoclave process and RFI. Finite element (FE) models of both panel types are developed and TSA is used to validate the models.

Keywords: Composite sandwich structure, RFI, TSA, full scale testing

INTRODUCTION

The recent increased use of composite sandwich structure in airframe construction has resulted in significant weight reduction; e.g. the Airbus A380 structure is made up of 22% from composites by weight, while the Boeing 787 is expected to be made from 50% composite structure [1]. However, the reduction in weight comes at a cost premium, as the production methods associated with the manufacture of composite sandwich parts are very expensive [2, 3]. Currently, the sandwich panels are produced by hand lay-up before being consolidated and cured in an autoclave. The inherent disadvantages of the hand lay-up/autoclave process have been discussed [2, 4]. It has been shown in previous work [3] that significant savings can be made if the conventional process is replaced with resin film infusion (RFI). It was also shown that there was no significant reduction in the properties of the face sheet material for both processes. In practice the materials will be employed in a sandwich panel and it was considered that, to fully assess the performance of the material, some full scale tests were required. In previous work a generic panel has been designed that is representative of secondary wing structure for use in full scale testing (see Figure 1) [3, 5]. The panel incorporates some of the features present in secondary wing structure, such as sandwich construction with honeycomb core and quasi-isotropic face sheets, whilst remaining simple enough to ensure it is possible to compare manufacturing processes and not be distracted by stress concentrations resulting from design features.

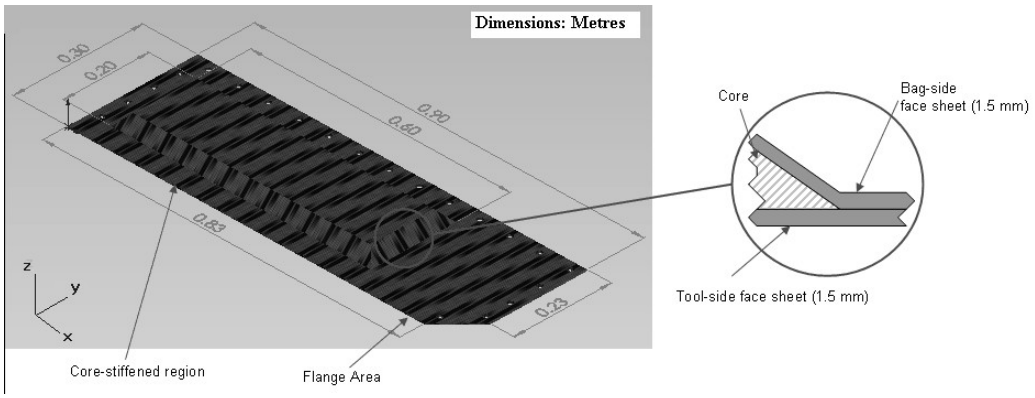

Figure 1: Generic panel design

The work described in the current paper considers the next step in the measurement of the performance of panels produced using the conventional autoclave process (M1) and RFI (M2). For this purpose generic panels manufactured from the two processes are tested using a custom built test rig that applies a pressure load which is representative of the service load (see Figure 2). The rig uses a standard servo-hydraulic test machine that pulls the generic panels over a water filled flexible cushion to apply a distributed pressure load on the panels. Full details of the design and commissioning of the rig and proof of its ability to apply consistent pressure loads whilst using full-field optical measurement techniques, such as thermoelastic stress analysis (TSA) can be found in [5]. The current paper describes the construction of finite element (FE) models of the generic panel, and their experimental validation. The experimental validation is based on TSA; details of the application of the techniques are provided in the paper. The TSA results from tests on generic panels manufactured from M1 are used to validate the FE model, and results from M1 and M2 are compared to investigate the effect of manufacturing the panel from M2 instead of M1.

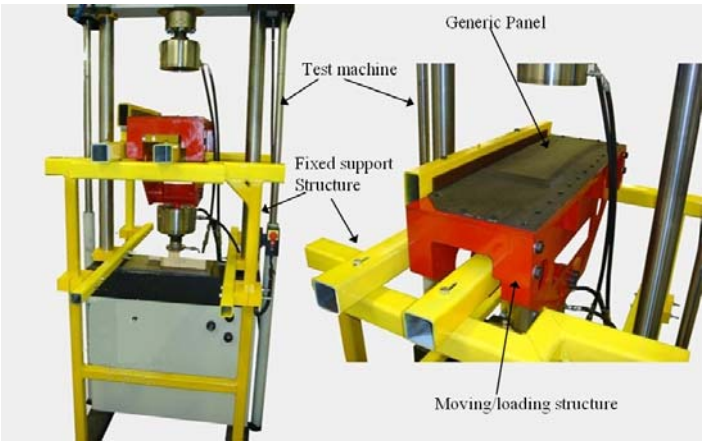

Figure 2: Pressure rig attached to test machine

FE MODEL

The FE model was constructed using ANSYS 11 (*ANSYS Inc, Canonsburg, USA*). Firstly, the flange region of the panel was constructed to include the plies of both the mould side

and bag side face sheets. Then the core was constructed by setting the size of the core that is touching the mould side face sheet and extruding in the z-direction (as shown in Figure 1). The chamfer on the core was produced by tapering in the x and y direction. The model was completed by adding the mould side face sheet plies to the base of the core volume and the bag-side face sheet plies to the areas on the top of the core. The fibre orientation was maintained on the angled edges of the core by altering the individual element coordinate systems such that z remained perpendicular to the surface. The core was assumed to be a single anisotropic solid volume with material properties as given in Table 1 it was modelled using eight node brick elements (Solid185) of 0.01 x 0.01 x 0.01 m. The carbon fibre face sheets were modelled using Shell181; a four node element suitable for producing layered FE models. The element can accommodate large linear rotations and large nonlinear strains, hence enabling the out-of-plane displacement of the panel to be derived. The ability of the element to allow a layered construction is also essential to enable the generation of a ply-by-ply model of the face sheets. Three models were produced: one with the face sheets modelled as the individual plies of M1, the second modelled the face sheets as homogenous orthotropic blocks with properties of M1, and finally modelling the face sheets as homogenous orthotropic blocks with properties of M2. The material properties used for the three models are provided in Table 1; the coordinates are shown in Figure 1.

Table 1: Material properties for FE models

Property	**Core**	**M1 individual ply**	**M1 Homogeneous**	**M2 Homogeneous**
$\mathbf{E_x}$ **(Pa)**	400×10^6	134×10^9	48.7×10^9	45.2×10^9
$\mathbf{E_y}$ **(Pa)**	400×10^6	9×10^9	50.4×10^9	46.7×10^9
$\mathbf{E_z}$ **(Pa)**	400×10^6	9×10^9	9×10^9	9×10^9
$\boldsymbol{\nu_{xy}}$	0.3	0.32	0.09	0.32
$\boldsymbol{\nu_{yz}}$	0.3	0.09	0.15	0.26
$\boldsymbol{\nu_{xz}}$	0.3	0.09	0.15	0.26
$\mathbf{G_{xy}}$ **(Pa)**	59.3×10^6	6.6×10^9	6.6×10^9	6.6×10^9
$\mathbf{G_{yz}}$ **(Pa)**	32.4×10^6	6.6×10^9	6.6×10^9	6.6×10^9
$\mathbf{G_{xz}}$ **(Pa)**	32.4×10^6	6.6×10^9	6.6×10^9	6.6×10^9

The service constraints were represented simply by imposing zero deflection on three edges of the model; i.e. the two short edges and one of the longer edges. With such boundary conditions, the model is constrained in all degrees of freedom along three edges, whilst the free edge has six degrees of freedom. A pressure load of 0.0103 MPa was applied to the model, equal to that used during the TSA tests, by applying a force perpendicular to each of the 2150 surface nodes. The pressure equates to a load of 0.96 N per node. The model is relatively thin in comparison to its length and width, and is subjected to an out-of-plane pressure load that would induce relatively large deflections. For this reason the model was solved using a geometrically nonlinear solver. Figure 3 shows the FE mesh alongside an example of the contour plot of the deflection of the model when subjected to a load of 0.0103 MPa.

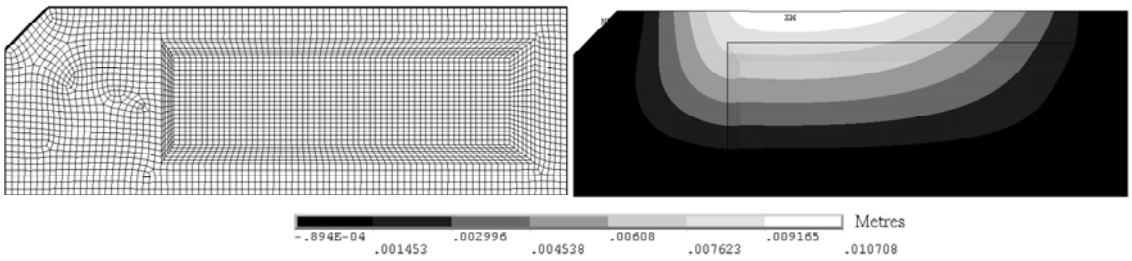

Figure 3: FE mesh and contour plot of out of plane deformation

EXPERIMENTAL WORK

The panels were loaded with the test rig described in the introduction. The response to the pressure applied to each of the generic panels was measured at a single point using a LVDT positioned at the region where the maximum out-of-plane deformation of the panel was predicted by the FE model (see Figure 3). This corresponds to a point approximately 160 mm from the top of the panel as shown in Figure 3. The displacement was recorded as the panel was loaded to 0.0103 MPa (1.5 psi). Once the displacement measurement was recorded a cyclic pressure was applied and TSA was used to capture data from the entire surface of the panel. A Cedip Silver 480M infra-red system was used to obtain the thermoelastic readings from the bag-side face sheet. As the panels were quite large (900 x 300 mm) it was necessary to take several TSA images across the surface of the panel. The Cedip camera was attached to a stand that prevented the vertical movement whilst allowing movement in the horizontal plane permitting data to be captured from 32 regions on the surface of the panel. Each TSA image was 320 x 256 pixels, to obtain adequate spatial resolution (0.3 mm/pixel) 32 separate images were collected. To join the images reference points that could be seen in the data were marked on each panel. The images were analysed manually to identify the joining lines. Then they were imported into Matlab as an array of temperature change values, one for each pixel, so they could be joined using a Matlab procedure developed for this purpose.

The output from the detector provides the change in surface temperature, ΔT, resulting from the change in the sum of the principal stresses on the surface of the material. For an orthotropic material, such as the composites considered in this thesis, ΔT can be related to the stresses in the material, σ_L and σ_T, as follows [6]:

$$\Delta T = -\frac{T}{\rho C_p}\left(\alpha_L \sigma_L + \alpha_T \sigma_T\right) \qquad \textbf{(1)}$$

where α_L and α_T, are the coefficients of linear thermal expansion in the longitudinal and transverse material directions, σ_L and σ_T are the stresses in these directions, ΔT is the change in temperature, T is the ambient temperature, ρ is the density and C_p is the specific heat at constant pressure. It is possible to combine the materials constants in this equation, i.e. α_L, α_T, ρ and C_p into two calibration constants K_L and K_T as follows [7]:

$$\Delta T = T\left(K_L \sigma_L + K_T \sigma_T\right) \qquad \textbf{(2)}$$

where $K_L = \frac{\alpha_L}{\rho C_p}$ and $K_T = \frac{\alpha_T}{\rho C_p}$.

The advantage of the form of the relationship in Equation (1) is that it is not necessary to obtain the thermal and mechanical properties, but instead the values of thermoelastic constants, K_L and K_T, can be obtained experimentally. The simple unidirectional stress state in tensile test specimens provides the ideal situation to derive the thermoelastic constants of a material. Strips of the face sheet material with surface plies at 0º for K_L and at 90º for K_T were manufactured and loaded in uniaxial tension at a level of 3.5 ± 3 kN. Equation (1) has been derived assuming adiabatic conditions, which are achieved by applying a cyclic load. Previous work [8] recommends that adiabatic conditions cannot be achieved at less than 15 Hz. However, it would be impossible to load at this rate using the test rig. Therefore, it was decided to use the 1 Hz loading frequency for the TSA work in the rig. As epoxy has a low thermal conductivity it was considered that this might be practical. Figure 4 shows the TSA images of both materials with surface plies at 0° and 90° and the thermoelastic constants calculated from these [5].

The generic panels were subjected to a mean load of 0.01 MPa (1.5 psi) with a range of pressure of approximately 0.01 MPa (1.5 psi) to the panel; the loading frequency was 1 Hz. The full field TSA data was processed into a form that can be compared with the FE. This was done by rearranging Equation (2) as follows:

$$\frac{\Delta T}{TK_L} = \Delta\sigma_x + \frac{K_T}{K_L}\Delta\sigma_y \qquad \textbf{(3)}$$

TSA **FE**

The TSA data is calibrated using K_L and then it is necessary to obtain σ_x and σ_y separately from the FE model. The stresses from the FE model are summed with a factor applied to σ_y of K_T/K_L. It should be noted that by calibrating the TSA data this way it can only be used to validate the homogeneous models.

The panels were subjected to a mean load of 0.01 MPa (1.5 psi) and then loaded in displacement control with 3 mm amplitude. This imparts a range of pressure of approximately 0.01 MPa (1.5 psi) to the panel; the loading frequency was 1 Hz.

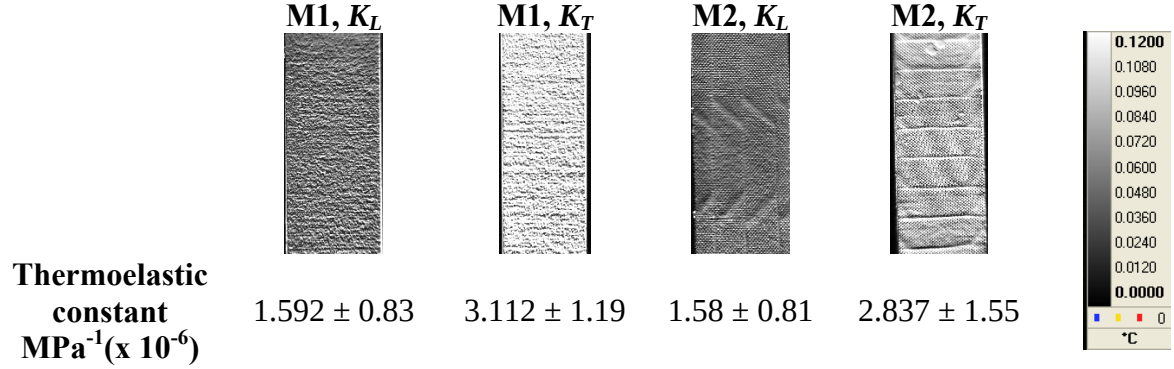

Thermoelastic constant $MPa^{-1}(x\ 10^{-6})$	1.592 ± 0.83	3.112 ± 1.19	1.58 ± 0.81	2.837 ± 1.55

Figure 4**:** TSA images to measure the calibration constants for each of the materials

MODEL VALIDATION

To initially validate the FE model, experimental results from panels produced using M1 were used. Considering the maximum out-of-plane deflection, measured experimentally by the LVDT transducer, the FE predicts 5.7 mm (individual ply model) and 7.7 mm (homogeneous model), but experimentally the deflection was measured as 6.34 mm. There is a large difference between the two FE models and with the individual ply model giving the closes reading, but not close enough to give confidence. The discrepancy can be attributed to the homogenous model not modelling the coupling that occurs in the actual off-axis laminate configuration. A simple calculation using classical laminate theory (CLT) [9] highlights the omission in the homogeneous model. The homogeneous model cannot account for the torsional coupling that relates the moments to curvature in the panels. To confirm this, FE models were produced with a cross ply lay-up, i.e. no torsional coupling. These provided the maximum out-of-plane deflection of 7.112 mm for the homogeneous model and 7.126 mm for the ply-by-ply model. To confirm this experimentally a cross ply panel was produced using the M1 and this deflected by 7.03 mm. This goes someway to explaining the difference in the predicted deflections for the two different model types and demonstrates that it is essential to develop a ply-by-ply model to avoid conservative predictions of deflection.

The stress prediction from the homogeneous FE model was validated using TSA. The FE data was processed into the form given by Equation (3). Figure 5a shows the processed stress data for the homogeneous model of M1. Figure 5b contains an example of processed TSA images of panels M1. In these images, the brighter circles around the perimeter of the panels are the metal penny washers used to counteract the stress raiser around the attachment holes, which are not included in the FEA. On top of the core the two rows of rectangular patches at regular intervals are used to assist in the image joining process.

Qualitatively there is excellent agreement between the TSA and the processed predicted image from the homogeneous FE model. The experimental results correspond well to the FE model stress fields, confirming the way the stresses are distributed in the panel. There is a comparatively small level of stress in the majority of the panel, and the position of stress concentrations at the corner junction of the foam core and the flange is confirmed. Around the boundary it can be seen that the larger stresses predicted by the FE model are apparent in the experimental data but a quantitative comparison is impossible because of the holes have not been included in the FE model. To provide a quantitative comparison between the results from the FE model and the TSA, a line of data was obtained horizontally across from left to right through the stress concentration at the corner of the core and is given in Figure 6 for both data sets. The FE data is from the homogeneous model. There is excellent agreement in the position of the stress peak, and the shape of the curve of the stress immediately around the peak. The stress gradually builds up across approximately 100 mm of the non-stiffened flange region and peaks at the junction between non-stiffened and stiffened areas. The stress rapidly reduces across the core stiffened

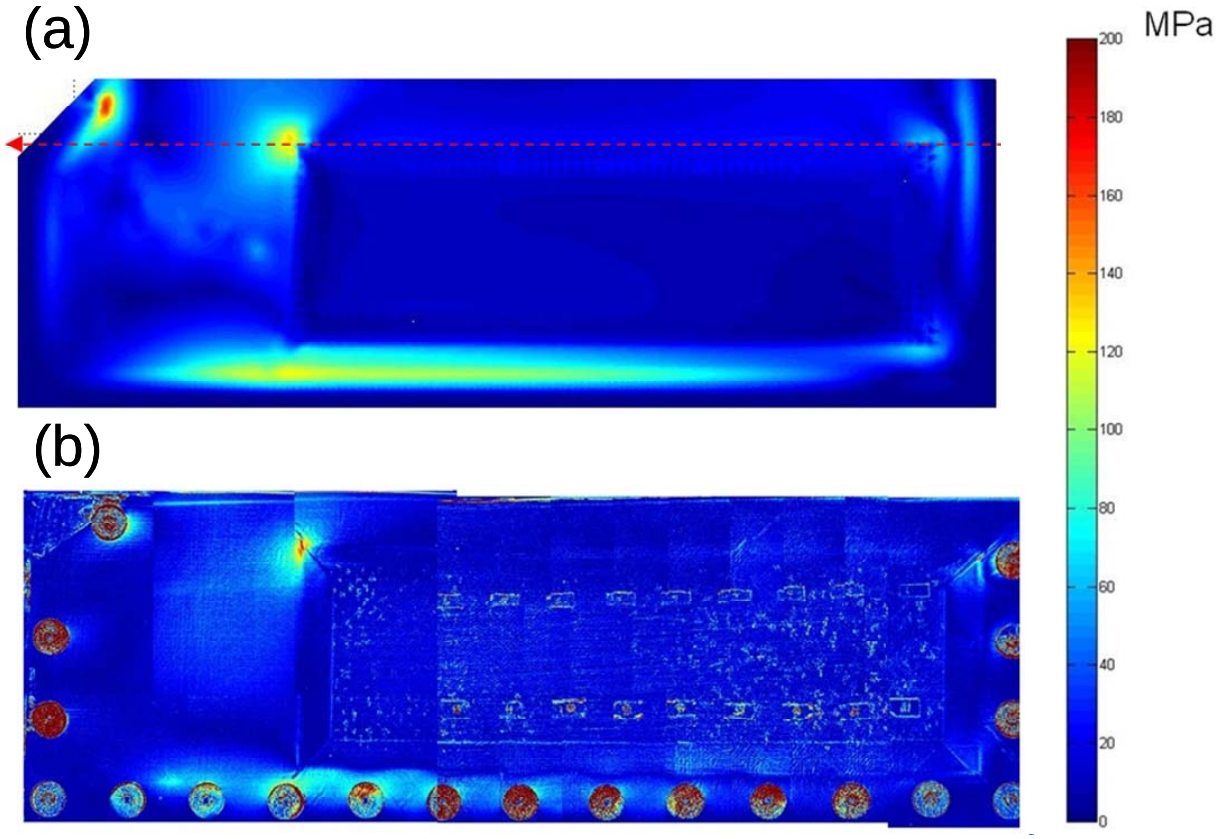

Figure 5**:** (a) Processed stress data from FE models using the homogeneous model, (b) Example of full-field experimental data from M1

region until it settles to a low, background level. This is intuitively correct, as the step increase in the flexural rigidity of the panel with the inclusion of the core would immediately reduce the stress. Although there is some noise in the TSA data it closely follows the FE data, and peaks at exactly the same position. The FE predicts a peak value of approximately 130 MPa, but the TSA records a stress of around 160 MPa. This difference may be accounted for by the resolution of the FE model around the core corner, or also by some noise in the TSA. The element size was selected to avoid a model that was computationally too expensive. In future work the number of elements around the core edge will be increased to investigate if the differences in the peak values are due to some smoothing. The difference in stress distribution might be due to the use of the stress from the homogenous model over the individual ply one. This will be further investigated in future work. However, the plot in Figure 6 validates the FE model for use in stress prediction for the M1 material.

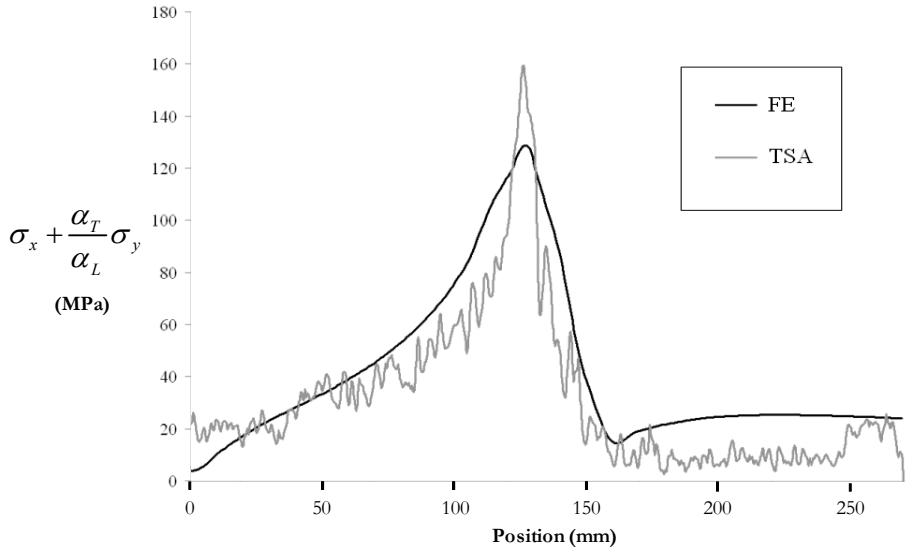

Figure 6: FE and TSA comparison for M1

The measured deflection for the panels manufactured from M2 was 4.6 mm. The FE model predicted 6.89 mm (for the homogeneous model); however it was not possible to produce an individual ply model due to the inherent quasi-isotropic nature of the raw material. By using the non-crimp fabric infiltrated using RFI in a conventional oven the maximum deflection was reduced by 27% over the baseline process, M1. Such a large reduction in deformation is significant, and could be due to the stitching in the NCF. Figure 7 shows a plot comparing the stress sum data through the stress concentration around the core from both TSA and FE of M2. The plot again shows agreement, however the noise from the stitching causes a deleterious effect, however it appears that the stress is better distributed in the face sheet than is predicted by the FE.

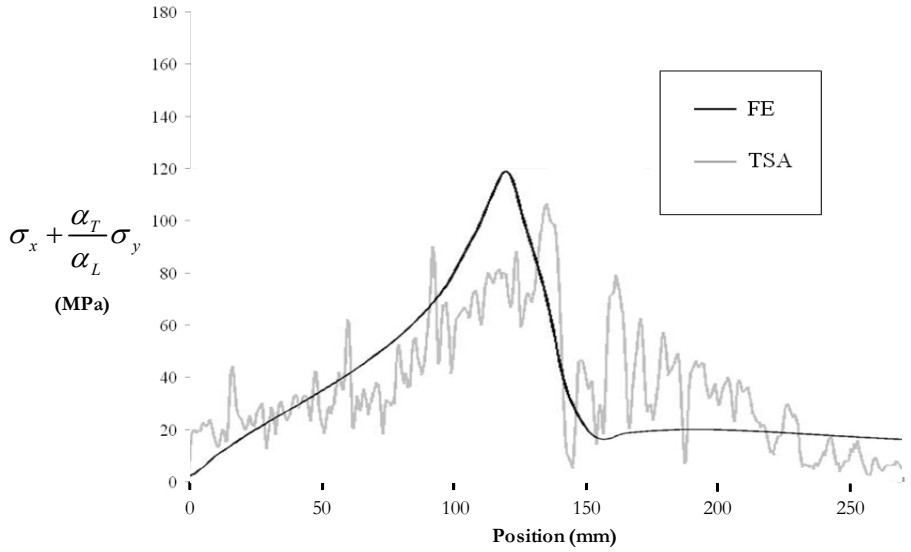

Figure 7: FE and TSA comparison for M2

Table 2 summarises the response of the generic panels produced using both materials M1 and M2. The experimental data was collected along 10 lines adjacent to the line used for the plots in Figures 6 and 7. The lines were spaced a pixel apart. The average peak value for the lines was obtained by finding the peak in each. The average to the left and right of the peak was obtained by, first, taking the average for each line, and then calculating the average of these. As the lines were space a pixel apart the averaging covers a small distance of 3mm.

In general the results in Table 2 show a good comparison between the TSA and FEA. The panel produced using M2 has a significantly reduced significantly reduced stress peak compared to M1. From mechanical characterisation tests on the face sheet materials [3] there was no significant difference between the flexural stiffness of M1 and M2. The full scale tests are showing that the different material has an effect. The noise in the TSA data is of a level that does not hinder the measurement of stresses in the panels, although the stitching in M2 does offer consistently greater noise than M1. The tests have offered some proof that the use of M2 process can be used to provide a panel with adequate, possibly improved, performance compared to M1 and successfully validated the models.

Table 2: Summary of experimental results for both materials

Material	$\left(\Delta\sigma_x + \frac{K_T}{K_L}\Delta\sigma_y\right)$ **(MPa)**		
	Left average	**Peak average**	**Right average**
1 (EXPT)	32.1 ± 9	178.0 ± 10 [191]	10.5 ± 10
1 (FEA)	25.0	130.0	7.0
2 (EXPT)	29.2 ± 12	122.0 ± 12 [136]	21.3 ± 19
2 (FEA)	19.0	118.0	3.0

CONCLUSIONS

This paper contains a comparison of the mechanical performance of materials produced using two processes: first hand lay-up of UD prepreg cured in an autoclave (M1); and second resin film infusion (RFI) of non-crimp fabrics cured in an oven (M2). Full scale tests of sandwich panels provided the measured thermoelastic response which was used as a basis for the performance comparison . The thermoelastic data were also used to validate FE models of the generic panel, which compared favourably with the experimentally derived stress data. More importantly the results demonstrated the out-of-autoclave process (M2) is capable of producing sandwich structures that can provide adequate, if not an improvement in, mechanical performance for use in secondary wing structure.

REFERENCES

1. National Composites Network, **www.ncn-uk.co.uk**, 04/2008

2. Chestney, J.A. and Sarhadi, M. *A prototype manufacturing cell for automated assembly of fibre reinforced composite preforms*. In 4th international conference on Automated Composites. 1995. Nottingham UK Institute of Materials.
3. Crump, D.A., Dulieu-Barton, J.M and Savage, J. *The manufacturing procedure for aerospace secondary structure panels*. Journal of sandwich structures and materials. 2009, DOI: 10.1177/1099636208104531, p1-28 *In press*.
4. Abraham, D. and Mcllhagger, R. *Investigations into various methods of liquid injection to achieve mouldings with minimum void contents and full wet out*. Composite part A: Applied science and manufacturing. 1998. 28: p 533-539.
5. Crump, D.A., Dulieu-Barton, J.M., and Savage, J. *Design and commissioning of an experimental test rig to apply a full-scale pressure load on composite sandwich panels representative of aircraft secondary structure*. Submitted to Measurement, Science and Technology.
6 Dulieu-Barton, J.M., Quinn, S., Shenoi, R.A., Read, P.J.C.L., and Moy, S.S.J, *Thermoelastic stress analysis of a GRP tee joint*. Applied Composite Materials, 1997. 4(5): p. 283-303.
7 Boyd, S.W., Dulieu-Barton, Thomsen, O.T. and Gheradi, A., *A development of finite element model for analysis of pultruded structures using thermoelastic data*. Composites Part A: Applied science and manufacturing, 2008. 29: p. 1311-1321.
8 Crump, D. A. (2009). *Reducing the cost of manufacturing composite aircraft secondary structure*. School of Engineering Sciences, University of Southampton: EngD Thesis.
9 Daniel, I.M., Ishai, O., *Engineering Mechanics of Composite Materials*. 1994: Oxford University Press.
10 Johannes, M., Dulieu-Barton, J.M, Bozhevolnaya, E., Thomsen, O.T., *Characterisation of local effects at core junctions in sandwich structures using thermoelastic stress analysis*. The Journal of Strain Analysis for Engineering Design, 2008. 43(6): p. 469-492.